NANO · MICRO small
www.small-journal.com

An Ultrasound-Responsive Theranostic Cyclodextrin-Loaded Nanoparticle for Multimodal Imaging and Therapy for Atherosclerosis

Sourabh Mehta, Viktoria Bongcaron, Tien K Nguyen, Yugandhara Jirwanka, Ana Maluenda, Aidan P G Walsh, Jathushan Palasubramaniam, Mark D Hulett, Rohit Srivastava, Alex Bobik, Xiaowei Wang, and Karlheinz Peter**

In memory of Prof. Rinti Banerjee, who initiated the project but succumbed to COVID-19

Atherosclerosis is a major cause of mortality and morbidity worldwide. Left undiagnosed and untreated, atherosclerotic plaques can rupture and cause cardiovascular complications such as myocardial infarction and stroke. Atherosclerotic plaques are composed of lipids, including oxidized low-density lipoproteins and cholesterol crystals, and immune cells, including macrophages. 2-Hydroxypropyl-beta-cyclodextrin (CD) is FDA-approved for capturing, solubilizing, and delivering lipophilic drugs in humans. It is also known to dissolve cholesterol crystals and decrease atherosclerotic plaque size. However, its low retention time necessitates high dosages for successful therapy. This study reports CD delivery via air-trapped polybutylcyanoacrylate nanoparticles (with diameters of 388 ± 34 nm) loaded with CD (CDNPs). The multimodal contrast ability of these nanoparticles after being loaded with IR780 dye in mice is demonstrated using ultrasound and near-infrared imaging. It is shown that CDNPs enhance the cellular uptake of CD in murine cells. In an ApoE$^{-/-}$ mouse model of atherosclerosis, treatment with CDNPs significantly improves the anti-atherosclerotic efficacy of CD. Ultrasound triggering further improves CD uptake, highlighting that CDNPs can be used for ultrasound imaging and ultrasound-responsive CD delivery. Thus, CDNPs represent a theranostic nanocarrier for potential application in patients with atherosclerosis.

1. Introduction

Atherosclerosis is a chronic inflammatory disease of the large muscular and elastic arteries. It is commenced by the accumulation and oxidation of low-density lipoprotein (LDL) into the sub-endothelial space of large arteries normally containing a dysfunctional endothelium.[1,2] Early uptake of LDL by macrophages and vascular smooth muscle cells results in the development of fatty streaks, which may progress to high-risk atheromas containing large amounts of oxidized-LDL (ox-LDL), cholesterol crystals (CCs), macrophages, vascular smooth muscle- and macrophage-derived foam cells, and cellular debris, covered by a fibromuscular cap.[1,2] Left undiagnosed and untreated, these atheromas can manifest into life-threatening cardiovascular complications such as myocardial infarction, and stroke.[2,3]

High vessel cholesterol levels together with plaque inflammation are necessary for the progression of atheromas to

S. Mehta, V. Bongcaron, A. Maluenda, A. P. G. Walsh, J. Palasubramaniam, X. Wang, K. Peter
Atherothrombosis and Vascular Biology Laboratory
Baker Heart and Diabetes Institute
Melbourne, VIC 3004, Australia
E-mail: xiaowei.wang@baker.edu.au; karlheinz.peter@baker.edu.au

The ORCID identification number(s) for the author(s) of this article can be found under https://doi.org/10.1002/smll.202200967.

DOI: 10.1002/smll.202200967

S. Mehta, R. Srivastava
Department of Biosciences and Bioengineering
Indian Institute of Technology Bombay
Powai 400076, India

S. Mehta, R. Srivastava
Indian Institute of Technology Bombay – Monash Research Academy
Powai 400076, India

S. Mehta, A. P. G. Walsh, J. Palasubramaniam, X. Wang, K. Peter
Department of Medicine
Monash University
Melbourne, VIC 3004, Australia

V. Bongcaron, A. P. G. Walsh, J. Palasubramaniam, X. Wang
Molecular Imaging and Theranostics Laboratory
Baker Heart and Diabetes Institute
Melbourne, VIC 3004, Australia

complex rupture-prone plaques.[2,4] One of the common strategies in managing atherosclerosis is to lower LDL and cholesterol. Various lipid-lowering drugs such as statins, recombinant high-density lipoproteins, PCSK9 inhibitors, and high-density lipoprotein-mimicking molecules are used to treat atherosclerosis.[5–10] However, many of the drugs in use have significant side effects, e.g. statin-associated muscle symptoms.[11] Additionally, the limited efficacy of such drugs in facilitating atherosclerotic plaque reduction may explain the residual risk associated with atherosclerosis and the many deaths worldwide.[12] Early preclinical studies suggest that delivery of drugs using target-specific nanoparticles (NPs) rather than systemic delivery of free drugs greatly improves their anti-atherosclerotic efficacy.[13] To avoid the potential toxicity of drugs, non-drug molecules such as nanocarrier systems and cyclic sugars have been successfully utilized.[14,15]

Various derivatives of cyclodextrin, including β-cyclodextrin, γ-cyclodextrin, and 2-Hydroxypropyl-beta-cyclodextrin (CD), 2-Hydroxypropyl-gamma-cyclodextrin, are known to form an inclusion complex with hydrophobic molecules and to improve the solubility of hydrophobic molecules including cholesterol.[16,17] Recent studies have shown that among all cyclodextrin, 2-Hydroxypropyl-beta-cyclodextrin (CD) exhibits the highest affinity toward cholesterol and is pharmaceutically approved as excipient by various regulatory agencies for increasing the solubility of hydrophobic drugs and other applications[18,19] and is now approved for treating diseases such as Niemann–Pick type C1 disease,[18,20] were cholesterol metabolism is dysfunctional.[17] A recent study has shown that CD stabilizes atherosclerotic plaques by activating reverse-cholesterol efflux pumps. Thus, CD has enormous promise for treating cholesterol-driven diseases. However, treatment limitations exist, such as poor pharmacokinetics (the blood half-life is shorter than 1 h in mice, rats, and humans[21]) necessitating the use of high doses of CD to achieve the desired therapeutic effect and exposing dose-dependent side effects such as hearing loss. Sustained and local release of CD would likely improve its therapeutic efficiency and reduce side effects. To this end, an attempt was made to polymerize CD using carboxyl-to-amine conjugation chemistry to reduce the size-dependent renal clearance of free CD and improve its anti-atherosclerotic efficacy.[14] Further, to improve both retention time and anti-atherosclerotic effects, polymerized CD was complexed with statins and incorporated into a liposome nanocarrier for controlled delivery of CD and statin to the atherosclerotic plaque.[22] Similarly, to improve the loading and controlled release of rapamycin, acetylated-cyclodextrin-loaded Polyvinyl alcohol NPs were also developed for reducing atherosclerotic plaque size.[23] While such NPs exhibit greater efficacy against atherosclerosis compared to free drugs, they cannot be used for diagnostic applications in their described formulation. Hence, we have developed a theranostic NP using polybutylcyanoacrylate (PBCA) to be used for both CD delivery and ultrasound (US) imaging.

N-butylcyanoacrylate (BCA) is a butyl ester of 2-cyano-2-propenoic acid. The material is biocompatible, biodegradable, and commercially used as tissue glue.[24,25] The material polymerizes upon contact with water. Recently, BCA was used for making NPs and microbubbles for both drug delivery and biomedical imaging.[26,27] Methods require an acidic pH (pH 2.5 to 5) for the synthesis of BCA NPs,[28,29] which limits its application as a biotherapeutic molecule carrier or acidic pH-sensitive material. To resolve this problem, we have successfully developed a BCA NP using distilled water with air in its core. In this study, we first developed a one-step, one-pot method for the synthesis of air-trapped BCA NPs using distilled water. When injected into mice (**Figure 1**), the NPs showed echogenicity and carried sufficient near-infrared (NIR) dye for NIR optical imaging. Further, 2-Hydroxypropyl-beta-cyclodextrin-loaded polymeric nanoparticles (CDNPs) injected into atherosclerotic ApoE$^{-/-}$ mice showed a greater reduction in total plaque size compared to mice treated with free CD. Thus, CDNPs can be used as theranostic particles, as illustrated, to treat atherosclerosis and for multimodal contrast imaging.

2. Experimental section

2.1. Synthesis of NPs

2.1.1. Synthesis of BCA NPs (NPs)

Polymeric butylcyanoacrylate (PBCA) NPs were synthesized by adding (1% v/v) BCA (BOC sciences, BOCSCI Inc., NY, USA) to distilled water (DW) containing 1% TWEEN 20, TWEEN 80, or Triton X-100 (Sigma–Aldrich, USA). The sample was sonicated for 90 s of elapsed time (with pulsed time 10 s on, 20 s off) at 50 A in an ice bath.

2.1.2. Purification and Storage of NPs

The synthesized NPs were purified by centrifuging the processed solution at 1000 RCF (Eppendorf 5810R) for 10 min at

T. K. Nguyen, M. D. Hulett
Department of Biochemistry and Chemistry
La Trobe Institute for Molecular Science
La Trobe University Melbourne
Melbourne, VIC 3083, Australia
Y. Jirwanka
Toxicology Division
National Institute for Research in Reproductive and Child Health
Parel 400012, India
A. Bobik, K. Peter
Department of Immunology
Monash University
Melbourne, VIC 3004, Australia
A. Bobik
Vascular Biology and Atherosclerosis Laboratory
Baker Heart and Diabetes Institute
Melbourne, VIC 3004, Australia
X. Wang, K. Peter
Department of Physiology
Anatomy and Microbiology
La Trobe University
Melbourne, VIC 3083, Australia
X. Wang, K. Peter
Department of Cardiometabolic Health
University of Melbourne
Melbourne, VIC 3052, Australia

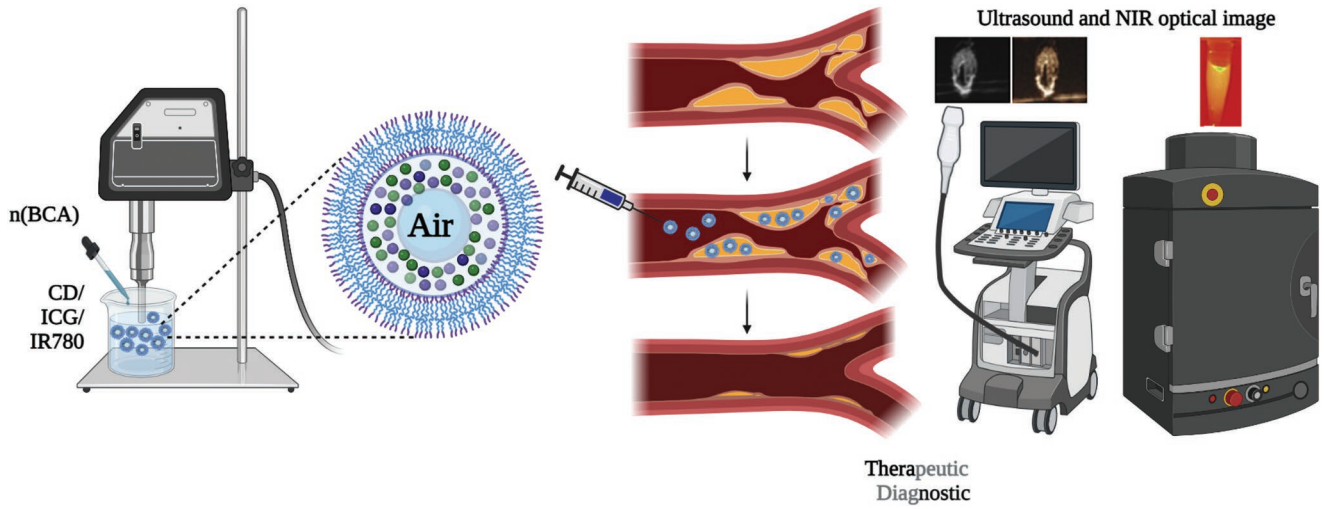

Figure 1. Theranostic nanoparticles (NPs) synthesized using *n*-butylcyanoacrylate (BCA). Air trapped NPs were synthesized using the sonication-based mini-emulsion method. The monomer BCA is emulsified in the aqueous phase and loaded with 2-hydroxypropyl-beta-cyclodextrin (CD) and indocyanine green (ICG)/IR780 dye. During the generation step, air is being trapped in the NPs. Intravenously injected CD-loaded NPs will accumulate at the atherosclerotic plaque and release CD, which reduces plaque size. The ICG/IR780-loaded and air-trapped NPs provided contrast enhancement via NIR fluorescence and ultrasound imaging. The generated theranostic NPs allow both the identification/diagnosis of atherosclerosis and effective anti-atherosclerotic therapy.

RT. Purified floating NPs were collected and resuspended into fresh DW or PBS and stored at 4 °C until further use.

2.1.3. Synthesis of CD/IR780/ICG-Loaded NPs

For synthesis of CDNPs, IR780 NPs, and indocyanine green (ICG) NPs, 150 µg mL^{-1} CD purchased from Cayman Chemical (Michigan, USA), 40 µg mL^{-1} IR780 dye (Sigma–Aldrich, USA), and 40 µg mL^{-1} ICG (MP Biomedicals, Solon, OH) solution with 1% TWEEN 20 were prepared, respectively. The NPs were synthesized by addition of BCA (1% v/v) via sonication, purified, and stored for further use.

2.1.4. Synthesis of NR-CD Complex-Loaded NPs

For the preparation of Nile Red-CD complex NPs (CD-NR NPs), first an NR-CD complex (CD-NR) solution was prepared by adding 200 µg NR (dissolved in 1 mL ethanol) to 150 mg mL^{-1} CD solution. The solution was stirred for 24 h to evaporate ethanol from the solution. The CD-NR solution was filtered using a 0.2 µm membrane filter. The CD-NR NPs were synthesized using a CD-NR solution of 1% TWEEN 20 and BCA (1% v/v) via sonication. The CD-NR NPs were purified and stored for further use.

2.2. Characterization of NPs

The synthesized NPs were characterized in relation to dispersity, hydrodynamic size, and surface charge using a Zetasizer ultra (Malvern Panalytical, Malvern, UK). Further, the structural features of the CDNPs were studied using transmission electron microscopy (TEM) images of the CDNPs obtained with a field emission gun transmission electron microscope (JEM 2100F, JEOL, Tokyo, Japan). The electron micrograph was obtained using brightfield mode at 120 kV.

The loading of CD into NPs was quantified using ^{1}H nuclear magnetic resonance (NMR) (Bruker Advance 600 MHz NMR Spectrometer).[30] A known amount of CDNPs was freeze-dried and then the CDNPs were dissolved in acetone. The acetone was evaporated overnight and a further 1 mL of deuterated (heavy) water (D_2O) was added to dissolve the entrapped CD. The solution was centrifuged at 2000 RCF using a centrifuge (Eppendorf 5810R) for 10 min at room temperature (RT) and the supernatant was collected for NMR analysis. For the quantification of CD, the CDNP samples and samples of the CD standard curve were injected into an NMR tube and placed in the Bruker Advance 600 MHz NMR Spectrometer. Maleic acid was used as the internal standard for quantification.[30]

2.2.1. In Vitro Pharmacokinetics of CDNP

We synthesized the Nile red-CD (NR-CD) complex by adding and stirring 1 mg mL^{-1} NR into 100 mg mL^{-1} CD for complex formation overnight. Next, we synthesized NR-CD complex-loaded particle. The entrapment efficacy of NR-CD was determined by particle destruction using Acetone and centrifugation to remove the polymer. The remaining solution was stirred overnight to evaporate the acetone from NR-CD complex solution and further quantified using UV–vis spectrometer. The particles and an equal amount of free NR-CD complex were added into the PBS at pH 7.4. The defined amount of PBS was collected at predefined time points and replaced with fresh PBS. The released NR-CD quantified against the standard curve of NR-CD complex. For estimating NR-CD release, we used the following formula:

$$\%\,\text{NR}-\text{CD released} = \frac{(\text{Abs. of NR}-\text{CD in the release media})}{(\text{Abs. of NR}-\text{CD entrapped into NP})} \times 100 \quad (1)$$

2.3. Primary Cell Culturing and In Vitro Experiments

Primary cell culturing of murine fibroblast cell lines (L929) and THP-1 monocytes were maintained in Dulbecco's Modified Eagle Medium and Roswell Park Memorial Institute 1640 (RPMI 1640) medium, supplemented with 10% FBS and 1% antibiotics (penicillin and streptomycin). Cells were kept at 37 °C in a humidified 5% CO_2 incubator.

2.3.1. In Vitro Biocompatibility

MTT assay was used to test the effect of the CDNPs on cell viability. 1×10^4 L929 cells were seeded into a 96-well plate to create a monolayer. After 24 h, the medium was replaced by a fresh medium containing 1×10^5 (800 pg mL^{-1} polymer) to 1×10^{12} CDNP mL^{-1} (0.8 mg mL^{-1} polymer). After 48 h, the cells were subjected to an MTT assay. The intensity of the developed purple color was measured using a multiplate reader (Varioskan Flash, Thermo-Fisher, USA) at 570 nm. To assess cell survival, optical densities were normalized to a 100% cell viability control (cells with no NP treatment).

2.3.2. In Vitro Cellular Uptake of NR-CD Complex-Loaded NPs

For study of the in vitro cellular uptake, L929 cells were seeded at a density of 5×10^4 cells well^{-1} into a 24-well plate and incubated for 24 h. 1×10^8 CD-NR NPs (0.8 µg mL^{-1} polymer) and an equal amount of free CD-NR, along with a nucleolus stain dye, Hoechst 33 342 (Thermo Fisher, USA), diluted in cell medium, were added to the wells. After 3 h of incubation, the treatment medium was removed from the cells, washed three times with PBS, and fixed with 4% formaldehyde for 15 min. The cells were then washed with DW three times and imaged using a confocal fluorescence microscope (CSU-X1, Yokogawa Electric Corporation, Japan). Cellular uptake was quantified using Image J version 1.5q (NIH, USA). Further, to understand the mechanism of cellular internalization, cells were pretreated with metabolic and various endocytic inhibitors (0.1% sodium azide and 2 µg mL^{-1} nystatin, 10 µg mL^{-1} phenothiazine, 24 µg mL^{-1} cyclosporin-A, and 4 µg mL^{-1} colchicine) for 1 h.[31] The spent medium was replaced with fresh medium containing CD-NR NPs and further incubated for 1 h. The cells were washed, fixed, and imaged using an epifluorescence microscope (EVOS M7000, Thermo Fisher, USA).

2.3.3. In Vitro Hemolysis Study

Human blood was collected from healthy volunteers, in compliance with the relevant laws and institutional guidelines, as approved by the Baker Heart and Diabetes Institute, Melbourne, Australia (Alfred Human Ethics, Project No: 627/17). Informed consent from the volunteers was obtained. Whole blood was incubated with 1×10^{11} NPs mL^{-1} (0.08 mg mL^{-1} polymer) for 1 h and 24 h at 37 °C at 150 rpm. After incubation, the samples were centrifuged for 5 min at 3000 rpm using a benchtop centrifuge (Eppendorf 5427R). Hemolysis was quantified by measuring the absorbance of the blood plasma at 550 nm using a UV–vis spectrometer (EnSpire Multimode Plate Reader, Massachusetts, USA). The hemolysis percentage was calculated using the following formula; PBS (pH 7.4) was used as the negative control and Triton X-100 was used as the positive control:

$$\%\,\text{Hemolysis} = \frac{(\text{Abs. of test sample} - \text{Abs. of negative control})}{(\text{Abs. of positive control} - \text{Abs. of Negative control})} \times 100 \quad (2)$$

2.4. Animal Experiments

All animals were purchased and maintained as per the animal ethical guidelines, at the Baker Heart and Diabetes Institute, Melbourne, Australia, under Alfred Plus Alliance Animal Ethics Committee no. E/1967/2019/B.

For in vivo biodistribution and biocompatibility study, all animals were purchased and maintained as per the animal ethical guidelines, National Institute for Research in Reproductive and Child Health, Mumbai, India, under Animal Ethics Committee no. E/6/20.

2.4.1. In Vivo Biodistribution and Pharmacokinetics Study

C57BL/6 mice were injected with 100 µL of 1×10^{10} ICG NP (80 µg polymer) mL^{-1}. Blood, vital organs, and tissues were collected at predefined time points to study the in vivo pharmacokinetics of ICG NPs. The amount of ICG was quantified by measuring the absorbance at an 808 nm wavelength using a UV–vis spectrometer (EnSpire Multimode Plate Reader, USA). The ICG standard curve was used for analyzing the released ICG and blood plasma from untreated mice was used as a control. For estimating ICG release, we used the following formula:

$$\%\,\text{ICG released} = \frac{(\text{Abs. of ICG in the blood plasma})}{(\text{Abs. of ICG entrapped into NP})} \times 100 \quad (3)$$

Organs were imaged using an optical imaging machine (IVIS Lumina Series III, Perkinelmer, USA) at 780 nm excitation wavelength and 808 nm emission wavelength. The images were processed using Living Image (Perkinelmer, USA) software and analyzed using Image J version 1.5q (NIH, USA).

2.4.2. In Vivo Compatibility Study

C57BL/6 mice were intravenously injected (via tail vein) with 100 µL of 5×10^{10} CDNP mL^{-1} (0.04 mg polymer mice^{-1}). After 48 h of injection vital organs- heart, lungs, liver, spleen, kidneys were collected to study the in vivo cytotoxicity. The organs were fixed with 10% formalin and sent to the local pathology lab in Mumbai, India for histology staining (Hematoxylin and Eosin). The stained organs and tissue were observed and analyzed using optical microscope (DM2000 LED, Leica, USA).

2.4.3. In Vivo Effects of CDNPs on Atherosclerosis

$APOE^{-/-}$ mice were used as a model of atherosclerosis. Male $APOE^{-/-}$ mice (6 weeks old) were placed on a high-fat diet containing 22% fat and 0.15% cholesterol (SF00-219, Specialty Feeds, Western Australia).[22,32] The mice were randomized and equally divided between the treatment group using 5×10^{10} CDNP mL^{-1} (0.013 mg/body weight/injection; considering average weight of mice was 30 g) and the two control groups: 5×10^{10} NP mL^{-1} (NPs only) (0.013 mg/body weight/injection, considering average weight of mice was 30 g) and an equal amount of free CD (CD only). The therapy or controls were administered via tail vein injection twice a week for 8 weeks. Post-treatment, their blood and entire aortas were collected. All samples were processed and analyzed in a blinded manner. Aortas were used for en face Oil Red O staining. The stained area was quantified using Image J version 1.5q (NIH, USA). Blood was centrifuged to collect plasma and plasma lipid profiling was performed at the Monash Pathology Lab using commercially available kits.

2.4.4. In Vivo US and NIR Fluorescence Contrast Imaging

C57BL/6 mice were anesthetized using a ketamine/xylazine cocktail, shaved, and placed on the 37 °C imaging station. The MS550 transducer operating at a frequency of 55 MHz was used with the Vevo2100 high-resolution imaging system (VisualSonics Inc., Toronto, Canada).[33] Briefly, the transducer was placed on the heart of the mouse to visualize the left ventricle. While imaging, 100 µL of 2.5×10^9 NPs (2 µg polymer) and IR780 NPs were injected via the femoral vein into the C57BL/6 mice. Real-time images were captured immediately, 1 min and 15 min post-injection. The same animals were imaged using an optical imaging machine (MiLabs, Netherlands) for in vivo NIR fluorescence imaging. The fluorescence was captured at a 780 nm wavelength by subjecting the mice to a 750 nm wavelength. The images were processed using Milab software and analyzed using Image J version 1.5q (NIH, USA).

2.5. Tissue-Mimicking Phantom for In Vitro US Imaging

A tissue-mimicking phantom cast was made using 1% agarose.[34] Molten agarose was poured into a container and a mold was inserted to form a variety of pockets. The agarose was left to solidify at RT and the mold was removed carefully. The agarose gel now had pockets/wells for loading our NPs using US imaging. Degassed water was added to fill the voids and keep the phantom hydrated until further use.

2.6. In Vitro US Imaging

An MS250 transducer operating at a frequency of 18 MHz was used with the Vevo2100 high-resolution imaging system (VisualSonics Inc., Toronto, Canada).[35] Videos and images were analyzed using linear contrast-agent imaging software (VisualSonics Inc., Toronto, Canada). In vitro US images were captured before and after loading the NPs into the predefined wells. The transducer was placed at 90 degrees to the properly loaded samples for recoding of US contrast enhancement.

2.7. In Vitro US-Triggered CDNP Cholesterol Reduction

For this experiment, the generation of cholesterol crystals (CCs) has been previously described.[1,36] We added NR to the CCs to create NR-CCs, and fluorescein isothiocyanate (FITC) to the CD to create FITC-loaded cyclodextrin complex (FITC-CD) NPs using the NR-CD complex synthesis method described above. The NR-CC-loaded macrophages were developed using a method described elsewhere.[1] Briefly, to make the NR-CC-loaded THP-1 macrophages, the cells were treated with 20 µg of NR-CCs for 4 h. Post-incubation, the cells were washed with PBS. The NR-CC-loaded macrophage cells were incubated with FITC-CDNPs and an equal amount of FITC-CD. The samples were treated with or without a US trigger (1 MHz, 2 W cm^{-2}, 50% duty cycle, and 30 s, i.e., 2.97 joules of US energy per mL of sample) using a sonoporator (SP100, Sonidel, Ireland). 3 h post-treatment, the spent medium was removed and the cells were washed with PBS to remove excess FITC-CD and FITC-CDNPs. The cells were observed and imaged using a confocal fluorescence microscope (CSU-X1, Yokogawa Electric Corporation, Japan). Next, CC-loaded macrophages and treated CC-loaded macrophage cells were stained with Oil Red O and the red color was quantified using a multiplate reader (Varioskan Flash, Thermo Fisher, USA) at 510 nm as described elsewhere.[37]

2.8. Statistical Analysis

Evaluation of outliers was performed using Grubbs' method. All data were expressed as mean ± standard deviation (SD). Sample size (n) has been included in the figure legend for each statistical analysis. Student's T-test or Mann–Whitney test were used for comparison between the two groups. One-way analysis of variance was used for comparisons between more than two groups, with Tukey's post-test. Differences were defined as significant when the p-value was $*p < 0.05$, $**p < 0.01$, $***p < 0.001$, or $****p < 0.0001$. Statistical analysis was performed using the Prism 9 (version 9.3.1; GraphPad Software, LLC. San Diego, CA, USA).

3. Results and Discussion

NPs enable size-dependent retention and accumulation of therapeutic molecules and improve the availability of hydrophilic molecules at cellular and systemic levels, thus ultimately enhancing the efficacy of drug delivery. Here we characterized a newly developed US-responsive polymeric NP, developed for theranostic applications in atherosclerosis.

3.1. Synthesis and Characterization of NPs and CDNPs

PBCA has been clinically used as a tissue adhesive.[25] The monomer n-BCA undergoes rapid anionic polymerization upon interaction with a hydroxyl group (OH). To control

polymerization, anionic polymerization inhibitors such as acidic aqueous phases have been typically used for generating PBCA NPs and microbubbles.[38,39] In this research, we used a non-acidic aqueous phase, distilled water (DW), which catalyzed the polymerization of BCA monomers to generate PBCA NPs. Probe sonication was conducted at the interface between the air and the aqueous phase, which not only generated local high mechanical shear, but also purged air into the emulsifying system, resulting in air-trapped PBCA NPs. As polymerization at low temperatures resulted in smaller particles,[39] we used an ice bath to control the polymerization temperature. We first optimized a one-step, mini-emulsion, anionic polymerization method to synthesize blank, air-trapped PBCA NPs (Figure S1a, Supporting Information). To optimize the synthesis parameters of the NPs, we systematically altered the surfactant, the sonication amplitude, and the elapsed sonication time. The synthesized NPs were centrifuged for 15 min at 1000 RCF at RT and the floating NPs were collected and stored at 4 °C or RT until further use. Dynamic light scattering measurements were performed to analyze the monodispersity of the samples using the polydispersity index (PDI) and then select the optimal parameters. The PDI reflects the distribution of size populations and a PDI less than 0.3 is considered acceptable and indicates a homogenous population.[40] Three surfactants were selected, and we found that NPs synthesized using TWEEN 20 had the lowest PDI of 0.25, compared to the use of Triton X-100 and TWEEN 80 (Figure S2a, Supporting Information). The surfactants were used to facilitate stabilization of the microbubbles, as well as to optimize the particle size distribution.[27] Next, we studied the effects of the sonication amplitude (A) in NP synthesis. Samples using 10, 30, and 50 A all resulted in PDI values lower than 0.3, with 50 A showing the lowest PDI of 0.18, indicating that the chosen amplitudes did not affect the monodispersity of the synthesized NPs (Figure S2b, Supporting Information). Using this amplitude of 50 A, we studied the effects of sonication times of 30, 90, and 180 s and found that the sample sonicated for 90 s elapsed time result in the best PDI of 0.18 (Figure S2c, Supporting Information).

Visually, we observed that the synthesized NPs floated (Figure S1b, Supporting Information), which could be attributable to their buoyancy due to the air that was trapped in the cores of the NPs during the synthesis process. In order to determine the potential of these NPs as an ultrasound contrast agent (USCA), we performed in vitro US imaging using a 1% agarose tissue-mimicking phantom. The echogenicities of the NPs in brightness mode (B-mode) images and contrast-enhancement mode (CE-mode) images were captured and analyzed (Figure S2d,e, Supporting Information). NPs synthesized using TWEEN 20 exhibited the highest contrast enhancement on US imaging compared to the other samples.

CDNPs were then synthesized, and TEM showed that they were spherical (**Figure 2**a,b). Under the microscope, the CDNPs were ≈388±34 nm in size (Figure 2b(i)), with a gas pocket in their cores. Figure 2b(ii) is a representative TEM image of

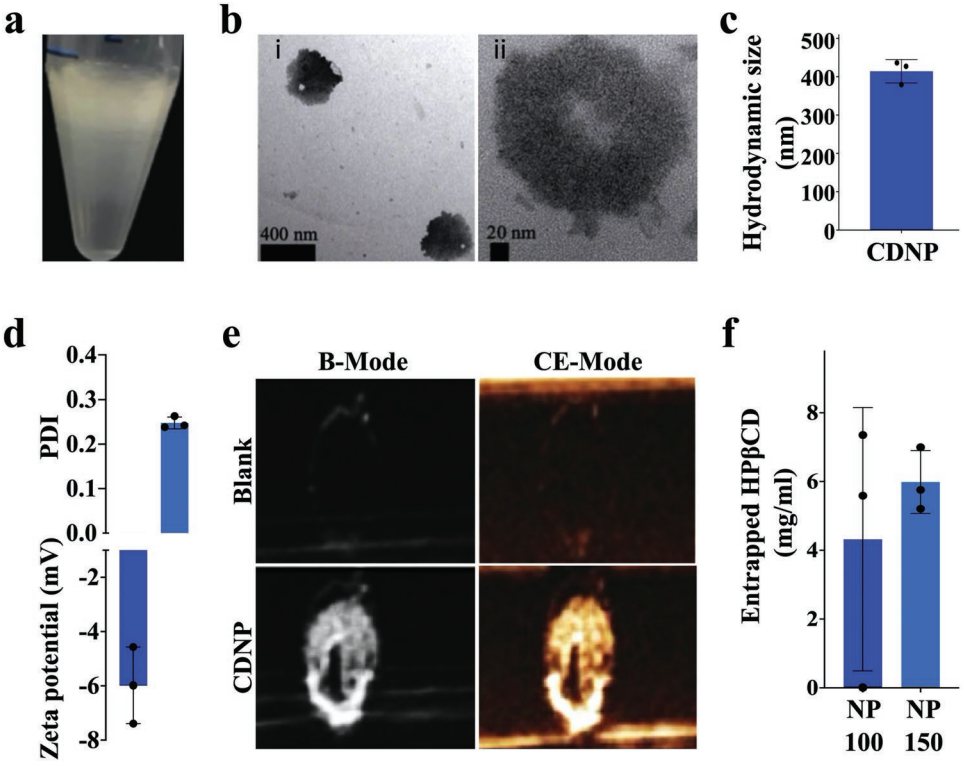

Figure 2. Synthesis and optimization of CD-loaded PCBA polymeric nanoparticle (NP) using non-acidic aqueous phase. a) CD-loaded polymeric nanoparticles (CDNPs) visible as a white layer on top, floating due to a buoyancy effect; b) TEM image of CDNP showing air cavity in its core; c,d) Measurement of hydrodynamic size, polydispersity index (PDI), and zeta potential of CDNP ($n = 3$), indicating the monodispersed nature of the synthesized CDNP; e) In vitro US imaging of CDNP indicating its echogenic nature; f) Quantification of entrapped CD in CDNP ($n = 3$, not significant). This assay was analyzed using the Mann–Whitney test. All data are presented as mean ± SD.

a CDNP showing the gas core, ranging in size from 19.35 to 45.16 nm, and a thick outer shell of PBCA with CD entrapped. Scanning electron microscopy (Figure S3, Supporting Information) showed that the CDNP has a spherical morphology similar to the transmission electron micrograph (Figure 2a). Using dynamic light scattering, the CDNPs in phosphate-buffered saline (PBS) (pH 7.4) had a hydrodynamic size of 413 ± 30 nm (Figure 2c) and PDI of 0.24 ± 0.01, and the zeta potential showed a surface charge of −5.990 ± 1.469 (Figure 2d). The CDNPs demonstrated stable hydrodynamic size, for up to 120 h, when stored at 4 °C and under room temperature conditions. However, as expected CDNPs showed a reduction in hydrodynamic size when stored at 37 and 40 °C, with 40% humidity in the stability chamber for the first 24 h, and then exhibited a relatively stable hydrodynamic size over 120 h (Figure S4, Supporting Information). Changes in hydrodynamic size at 37 and 40 °C could be due to polymer hydrolysis. The CDNPs had echogenic properties and could be visualized via US imaging using B-mode and CE-mode (Figure 2e). CD quantification using H^1 nuclear magnetic resonance (NMR)[39] showed that on average 5 mg CD was entrapped into 1×10^{10} NP mL^{-1} (Figure 2f). Further, we investigated the in vitro pharmacokinetics of CDNPs. For this study, we developed a Nile red CD (NR-CD) complex and generated NR-CDNP. We observed that 38% NR-CD complex was released in PBS (pH 7.4) from CDNP in the first 30 min at 37 °C. Over 48 h, we observed 100% release of NR-CD into the media (Figure S5, Supporting Information), indicating CDNP could be used for sustained and prolonged release of CD. The observed initial burst release in the first 30 min could be due to PBCA's biphasic degradation mechanism, in which rapid hydrolysis of ester side chains from the surface of the NPs resulted in the burst effect; followed by time-dependent hydrolysis driven by degradation of the polymer matrix of the NPs.[28,41,42] Hence, CDNP could be used for the controlled release of hydrophilic molecules such as CD.

3.2. NPs as Multimodal Contrast Agents

Real-time information about disease status plays a key role in designing personalized strategies against high-risk diseases such as atherosclerosis. Among all clinically approved diagnostic modalities, US is the most widely available and affordable imaging modality, and is considered the safest real-time diagnostic modality that provides information on the characteristics of the investigated tissue.[41–43,33,44] US contrast agents such as PBCA microbubbles (size >1 µm) have also recently attracted major interest and have been used to detect thrombosis and atherosclerotic plaques.[28,38] Our synthesized NPs exhibited US contrast enhancement and additional loading with NIR dye (IR780) resulted in the creation of a multimodal imaging reagent, as illustrated in Figure 1. First, we performed in vivo US imaging using an 18 MHz transducer (MS250) in the Vevo2100 high-resolution imaging system (VisualSonics Inc., Toronto, Canada). 100 µl of IR780 NPs (≈2.48×10^9) were injected into C57BL/6 mice via the femoral vein, as described previously.[45] US images were captured during the injection of the contrast agent in both B-mode and CE-mode. A real-time visual enhancement was observed in the left ventricle of the mouse heart as the NPs were injected (**Figure 3**a). Analysis of the contrast intensity showed an increase in signal as the agents entered the circulation. At 1 min post-injection, the NPs could be visualized via US in both B-mode and CE-mode. Their signal intensity returned to baseline after 15 min, indicating that our NPs can be used as US contrast agents in vivo. We then performed in vivo NIR fluorescence imaging (Figure 3b) and demonstrated that the intravenously injected NPs could be imaged using an optical scanner (MiLabs, Netherlands). The IR780 dye displays excellent NIR fluorescence activity and has also been used as a photoacoustic agent for diagnostic imaging of various cancer sites.[45,46] This proof-of-concept study indicates that the IR780 NPs can be used for multimodal US and optical imaging.

One of the limitations of the current NIR imaging technology is its depth limitation. This is one of the reasons why we have incorporated contrasts for both NIR and ultrasound in our dual contrast particle. Recent advances in the use of NIR dyes for photoacoustic imaging have been successfully used for imaging of carotid arteries in humans.[47] The use of dual-modality contrast particles provides the opportunity to pursue two complementary imaging approaches: For more superficial atherosclerosis, such as those in the carotid arteries, both NIR and ultrasound imaging can be applied, whereas, for deeper vessels and organs, ultrasound imaging remains the most reliable technology.

3.3. Stability of CDNPs as US-Responsive Agents

The echogenicity of the CDNPs was imaged at different dilutions. US visualization of these contrast agents was observed when using 1×10^5 CDNPs mL^{-1} but was drastically reduced when using 1×10^4 and 1×10^3 CDNPs mL^{-1} (Figure S6a, Supporting Information). To determine if US exposure had destroyed the CDNPs, they were subjected to continuous imaging for 10 min and images were captured every 2 min. Similar contrast-enhancement intensities were observed over the 10 min, indicating that the CDNPs remained intact and stable (Figure S6b, Supporting Information). For almost 10 min, we observed US in vivo in the liver (Figure S7, Supporting Information), indicating that NPs can be used as ultrasound contrast agents. To assess the storage stability of the CDNPs and the effects of storage on their echogenicity, they were stored at different temperatures (−80 °C, 4 °C, RT, and 37 °C) for 10 days. Post-storage, US imaging was performed, and we observed that the CDNPs maintained their echogenicity (Figure S6c, Supporting Information). A similar observation has been reported with PBCA microbubbles.[48] We freeze-dried CDNPs with 5% polyvinylpyrrolidone as a cryoprotectant for a longer storage time. The freeze-dried particles were reconstituted after 1 and 180 days of storage at RT. US imaging successfully visualized both samples of reconstituted CDNPs (Figure S6d, Supporting Information), indicating that the CDNPs could be stored for a prolonged time at RT; a similar trend has been reported for PBCA microbubbles.[48]

Therapeutic US using a high mechanical index to cause inertial cavitation and to burst ultrasonic particles has been employed to trigger US-responsive, site-specific drug delivery in various diseases including myocardial infarction.[49,50] To evaluate if our

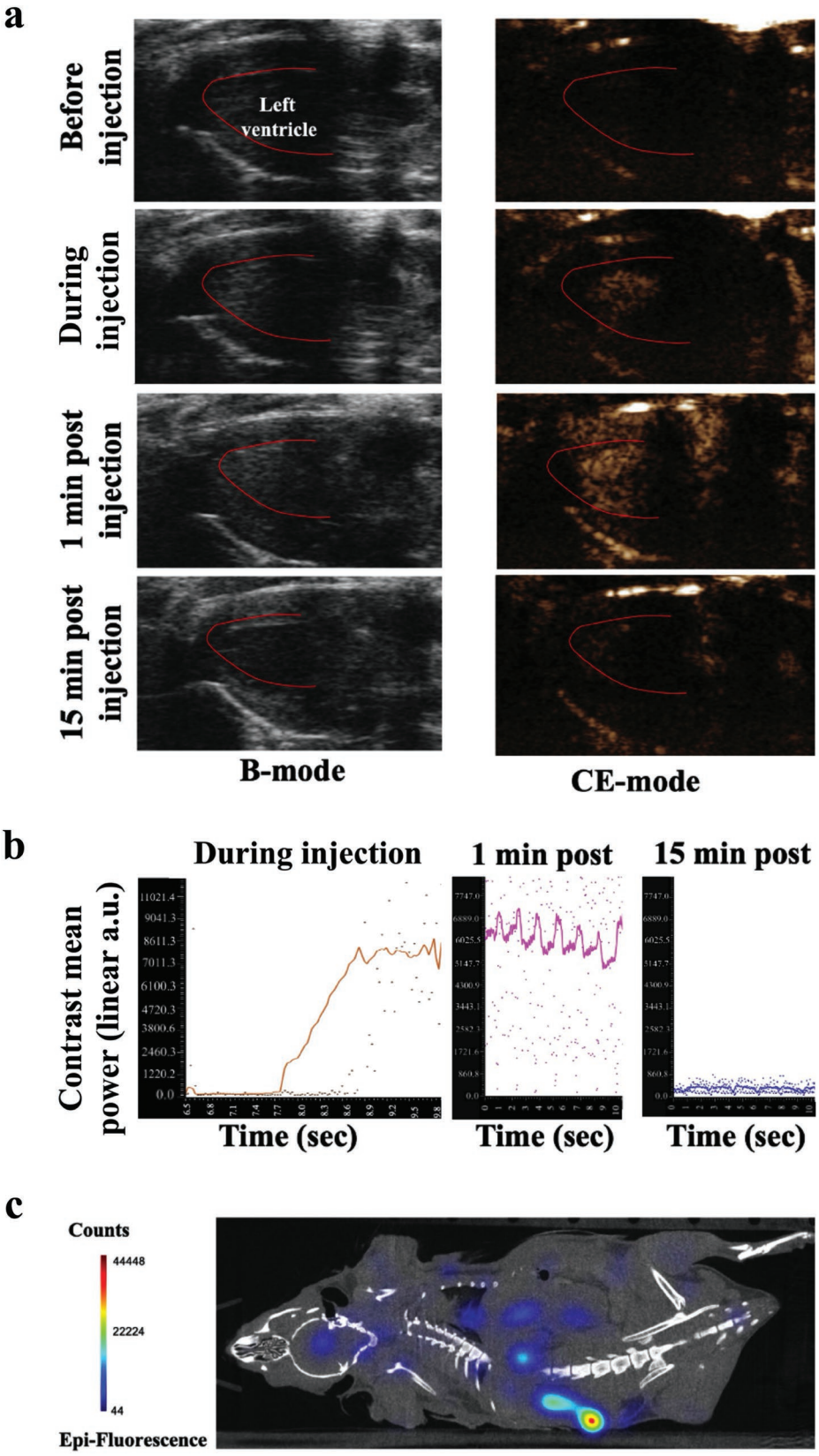

Figure 3. IR780 NP bimodal contrast agent for US/fluorescence imaging. a) In vivo US images showing contrast enhancement in B-mode and CE-mode in a mouse heart after intravenous injection of NPs, 1 min and 15 min post-injection; b) US contrast mean power (from Figure 3a) obtained during intravenous injection, 1 min and 15 min post-injection. c) In vivo NIR fluorescence image of mouse 20 min post-injection.

CDNPs underwent cavitation to release their drug load, we subjected them to a burst US mode (a predefined therapeutic mode of the Vevo2100 high-resolution imaging system, VisualSonics Inc., Toronto, Canada). US imaging pre- and post-burst application showed a loss of US contrast signal in vitro (Figure S6e,f, Supporting Information). The loss of signal intensity indicated that the CDNPs responded to therapeutic US by breaking and, hence, losing their echogenic property. During the burst, the drugs will be directly released into the targeted surrounding area.

3.4. In Vitro Cellular Interaction of CDNPs

The biocompatibility of the CDNPs was investigated using a murine fibroblast (L929 cell line) and MTT ((3-(4, 5-dimethylthiazolyl-2)-2, 5-diphenyltetrazolium bromide)) assay.[51] L929 cells were incubated with different concentrations of CDNPs ranging from 1×10^5 to 1×10^{12} CDNPs mL^{-1} for 48 h (**Figure 4**a). The biocompatible nature of the CDNPs was evident from the results of the MTT assay with at least 80% cell viability across all concentrations. To investigate the hemocompatibility of the CDNPs, we incubated them with human blood for 1 and 24 h. We observed no difference in hemolytic activity when compared with a PBS control, whereas a positive control using Triton X-100 showed 100% hemolytic activity (Figure 4b).

Next, in our in vivo biocompatibility study, we injected 5×10^{10} CDNPs mL^{-1} (0.04 mg polymer mL^{-1}), and after 48 h we observed no obvious toxicity in Hematoxylin and Eosin-stained vital organs such as heart, lungs, spleen, liver, kidneys under the microscope when compared with samples from the PBS treated group (Figure S8, Supporting Information). CDNP

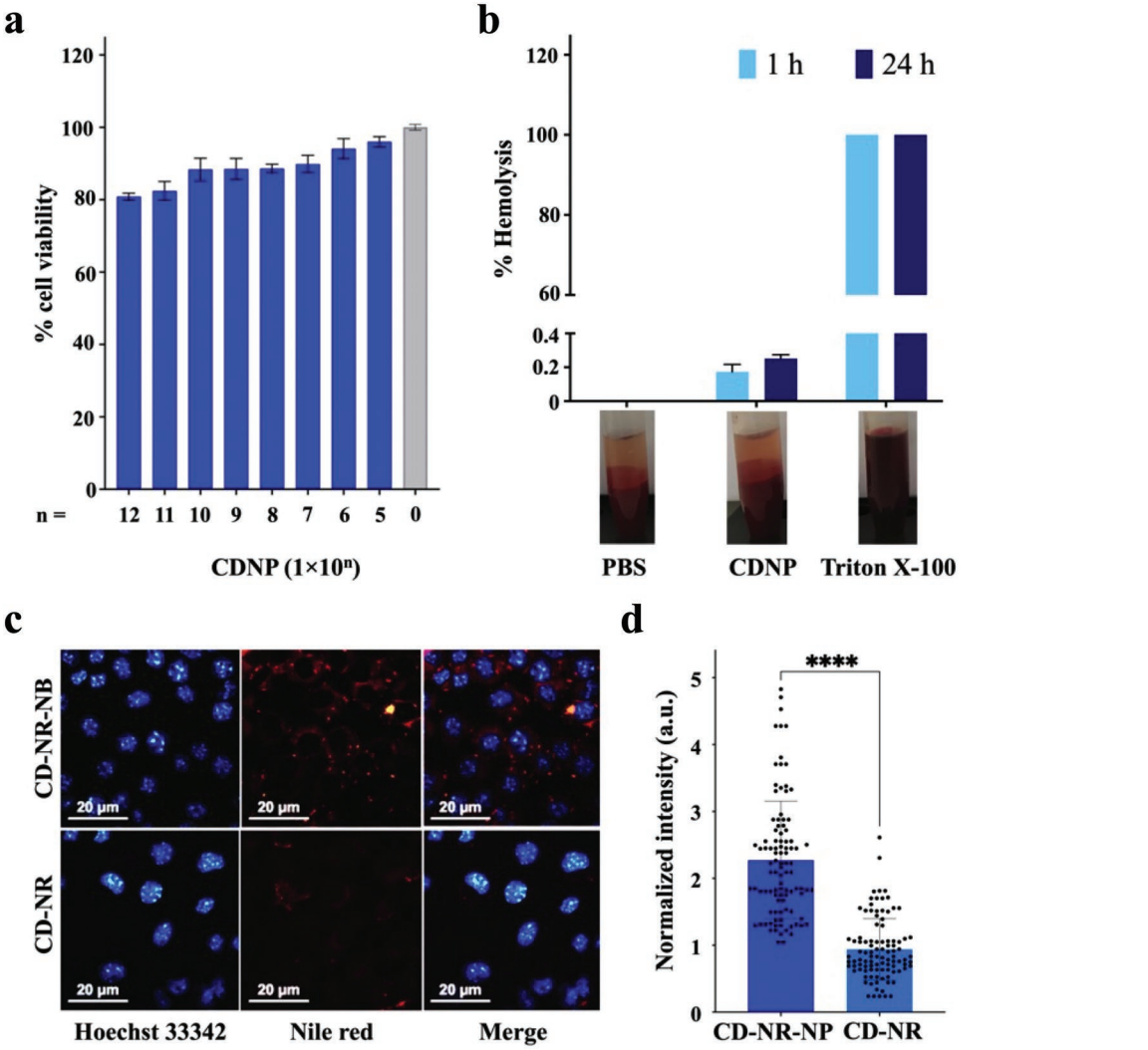

Figure 4. In vitro cellular interaction of CDNPs. a) In vitro biocompatibility of CDNPs on L929 cells, up to 1×10^{12} NPs mL^{-1} (0.8 mg polymer mL^{-1}) showing 80% biocompatibility ($n = 3$); b) In vitro hemolytic effect of CDNPs on blood samples ($n = 3$). Samples treated with PBS negative control were set as 0 and Triton X-100 positive control were set as 100%; c) In vitro cellular uptake of CD-NR NPs and CD-NR into L929 cells; d) Quantification of cellular uptake in L929 cells showing 2.41-fold fluorescence enhancement in CD-NR NP treated cells compared to free CD-NR treated cells ($n = 100$, $^{****}p < 0.0001$). Evaluation of outliers was performed using Grubbs' method; no data point was removed. This assay was analyzed using the Student's T-test. All data are presented as mean ± SD.

is made of clinically approved materials. CD is an approved excipient for pharmaceutical formulations,[52] and PBCA is clinically used as a tissue adhesive.[25] Hence, we expect that CDNP would show biocompatibility even at higher concentrations. Thus, we concluded that CDNPs are biocompatible and safe for in vivo use. L929 cells were also employed to study the cellular uptake of the CDNPs. We loaded a fluorophore, hydrophobic dye, Nile red (NR), into CD to generate CD-NR complexes (as CD forms an inclusion complex with hydrophobic molecules in its core bucket [17,50]), before generating CD-NR NPs. L929 cells were incubated with either CD-NR or CD-NR NPs for 3 h, followed by imaging via microscopy. Blue fluorescence using Hoechst 33342 staining represents the nuclei of the L929 cells, while red fluorescence represents the locations of CD-NR and CD-NR NPs; enhanced cellular uptake and internalization of CD-NR NPs compared with the free CD-NR were observed via fluorescence microscopy (Figure 4c). A 2.41-fold increase in fluorescence intensity was observed in the cellular uptake of the CD-NR NPs as compared to the free CD-NR (Figure 4d). This significant enhancement in the cellular uptake of CDNPs as compared to free CD can be attributed to receptor-mediated endocytosis. Further, the mechanism of internalization was studied using various endocytic blockers, and metabolic that is, nystatin, cyclosporine-A, phenothiazine, and colchicine, which respectively block the caveolae-dependent, calcineurin-dependent, clathrin-dependent, and microtubule-mediated endocytic pathways. The cells were pretreated with metabolic blockers and endocytic blockers as described by Chandan et al.[31] The cells pretreated with endocytic blockers showed weak fluorescence signals except for the colchicine-treated and cyclosporine-A-treated cells (Figure S9, Supporting Information). This indicates that the internalization of the CDNPs followed clatherine and caveolae pathways, but was independent of calcineurin and microtubule-mediated endocytosis. Similar trends were observed for the PBCA NPs. PBCA NPs seem to be subject to clathrin-mediated and caveolae-mediated endocytosis mechanisms.[53] Sodium azide (0.1%) was used as a metabolic blocker to block the synthesis of adenosine triphosphate. Cells pretreated with sodium azide showed more than 90% viability (Figure S10, Supporting Information). As no fluorescence signal for the sodium azide-treated cells were seen (Figure S9, Supporting Information), the internalization of the CDNPs seems to be an active process. These findings indicate that NPs improve the cellular uptake of CDNPs and thus the availability of CD in the cell cytoplasm.

3.5. In Vivo Biodistribution and Pharmacokinetics

The in vivo biodistribution and circulation of NPs depend in part on particle size, shape, material, surface chemistry, and charge.[54] To investigate their biodistribution and pharmacokinetics, we loaded indocyanine green (ICG) into our NPs to create ICG NPs (Figure S11a, Supporting Information). The ICG NPs emitted bright fluorescence at the 808 nm emission wavelength when exposed to 780 nm excitation, whereas the CDNPs and PBS, as expected, did not show any fluorescence, confirming that the ICG was entrapped in the ICG NPs and ICG CDNPs (Figure S11b, Supporting Information). The entrapment efficiency was measured as 36.30 ± 4.52% against the standard curve plotted for ICG (Figure S11c,d, Supporting Information).

For in vivo studies, we administered 100 µL of 1×10^{10} ICG NPs mL^{-1} (0.008 mg polymer mL^{-1}) intravenously into mouse tail veins. Blood was collected at a predefined time, then centrifuged to obtain plasma, and the ICG content was measured at 808 nm. Quantification of the ICG in the plasma showed the presence of ICG for up to 48 h with a peak at 1 h (**Figure 5**a). The presence of 30.34 ± 10.46% of ICG in the blood plasma in the first 30 min may have been due to released and adsorbed ICG from the surface of the ICG NPs or to rapid hydrolysis of ester side chains from the surface of the NPs. Plasma obtained in the first hour post-injection showed 64.91 ± 16.3% of ICG released and then gradually the concentration of ICG in the plasma decreased. Plasma collected 4, 24, and 48 h post-injection showed 41.74 ± 12.22%, 25.02 ± 15.15%, and 13.92 ± 9.56% of ICG, respectively. This release of ICG could have been due to time-dependent hydrolysis of the PBCA matrix, following its hydrolysis of ester side chains and time-dependent degradation of the polymer matrix of the NPs.[28,41,55]

Organ-specific in vivo biodistribution studies of the ICG NPs were performed using optical imaging using an excitation wavelength of 780 nm and an emission wavelength of 808 nm (Figure 5b,c). Imaging was performed on harvested organs and tissues (heart, lungs, liver, spleen, kidneys, and fat) that were harvested at different times of 1, 4, 24, and 48 h after administration (Figure 5c). The ICG NPs accumulated most extensively in the liver, followed by the heart and spleen, when compared with the untreated mice (the control). Fat tissue showed no or negligible fluorescence intensity (Figure 5b), suggesting that the NPs did not accumulate in fat. The in vivo biodistribution indicates that the NPs circulated in the blood of the mice for the first hour and were then accumulating in organs over 4 to 24 h.

3.6. CDNPs Improve Anti-Atherosclerotic Efficacy of CD

Advanced atherosclerotic plaques, similar to cancerous tumors, develop a leaky neovasculature, allowing NPs of sizes such as ours to accumulate and be retained.[22,56] This passive accumulation provides a homing or targeting effect to the atherosclerotic plaque and thereby represents a therapeutic targeting strategy. Hence, we expect our 388 ± 34 nm size CDNP to passively accumulate into the atherosclerotic plaque by size-dependent permeation and retention effect. CD is known to form inclusion complexes with cholesterol, thus enhancing the solubility of CCs in aqueous solutions ≈150 000-fold.[1] Recent studies of CD have shown its effectiveness in regression of atherosclerosis; peritoneally injected free CD (2000 mg kg^{-1}), twice a week, for 8 weeks of treatment in $ApoE^{-/-}$ mice showed 45% plaque reduction as compared to the control group.[1] Treatment with a statin–CD complex loaded onto NPs (CD 400 mg kg^{-1}) twice a week for 4 weeks resulted in ≈40% reduction in plaque area.[22] Our atherosclerotic $ApoE^{-/-}$ mice were treated with 5×10^{10} CDNP mL^{-1} (0.013 mg per body weight per injection) twice a week for 8 weeks and we observed significant regression of plaques in the CDNP-treated animals as compared to

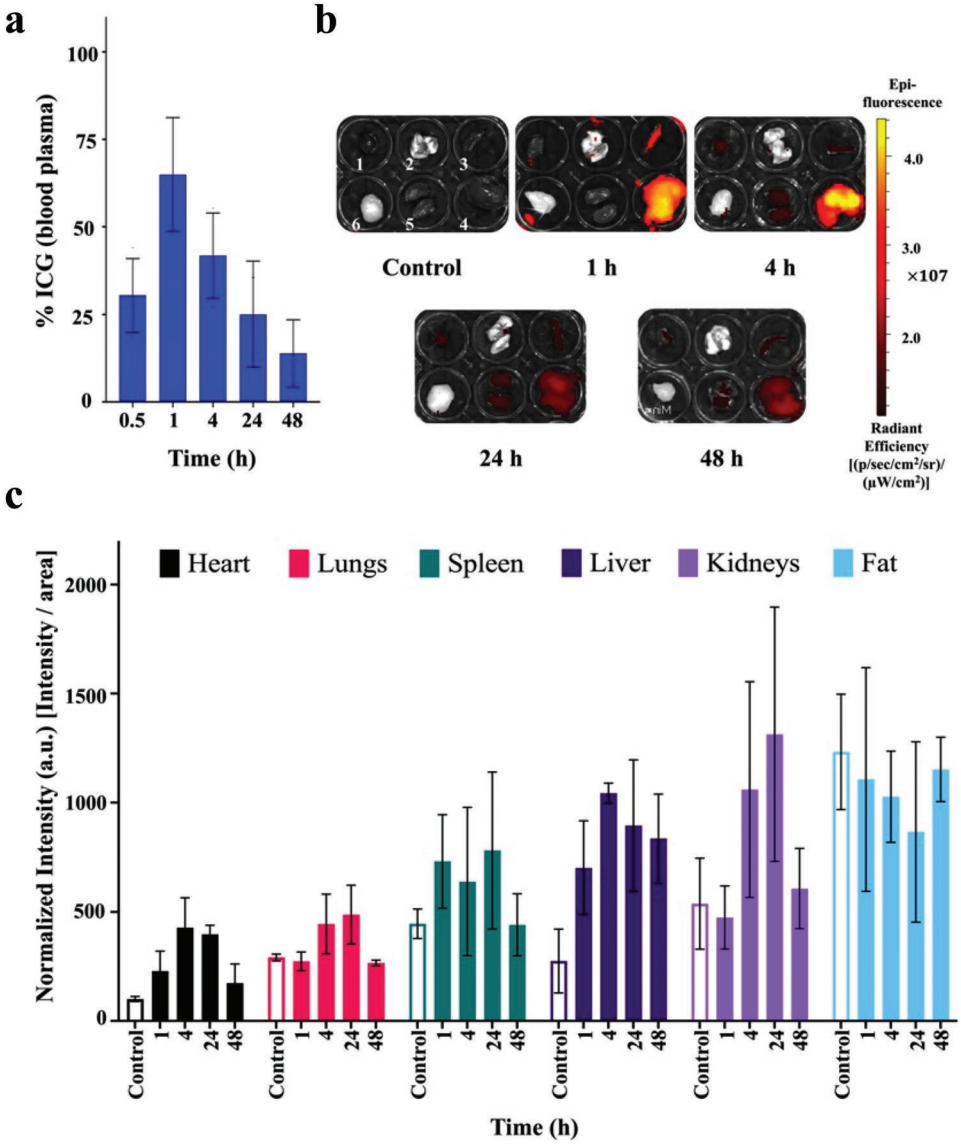

Figure 5. In vivo biodistribution and pharmacokinetics of ICG-loaded nanoparticles. a) In vivo pharmacokinetics of ICG-loaded NPs ($n \geq 4$); b) Representative ex vivo fluorescence images showing distributions of ICG-loaded NPs (1: heart, 2: lungs, 3: spleen, 4: liver, 5: left and right kidneys, 6: fat); c) Quantification of fluorescence intensities and compared with control group indicating NPs accumulated into various organs including the heart and very little or no NPs accumulated in fat ($n \geq 4$). All data are presented as mean ± SD.

the free CD-treated group via en face assessment of atherosclerosis in the aorta (**Figure 6**a; Figure S12, Supporting Information). Quantification of the en face Oil Red O-stained plaque area of the CDNP-treated group showed a significant reduction in total plaque area as compared to the animals treated with free CD and with NPs only (16.59 ± 3.42% vs 24.2 ± 4.19% vs 31.04 ± 4.44% respectively; $p > 0.01$; Figure 6b).

Mechanistically, CD solubilizes CCs from plaques and reduces the lipid burden by activating the reverse cholesterol efflux pump in macrophages, thereby reducing the plaque size, but CD does not seem to alter plasma cholesterol concentration.[1,57] The plasma lipid profiles demonstrated a significant reduction ($p < 0.05$) in the cholesterol levels in the CDNP-treated mice compared with blank NPs and with the free CD-treated mice (Figure 6c). No significant difference was seen in the plasma cholesterol levels between free CD and NP-treated mice, which is consistent with observations by Zimmer et al.[1] We observed a similar trend in the plasma very low density lipoprotein(VLDL)/LDL-cholesterol concentrations. A significant difference ($p < 0.05$) in the plasma VLDL/LDL-cholesterol concentrations (6.63 ± 0.90 mg dL^{-1}) was seen in the mice treated with CDNPs as compared to blank NPs (8.04 ± 0.90 mg dL^{-1}); however, the free CD-treated mice showed an average plasma VLDL/LDL-cholesterol concentration of 7.81 ± 1.25 mg dL^{-1}, which was slightly higher than that of the CDNP-treated mice (Figure 6d). This is in line with a recent study reporting that α-CD resulted in a reduction in plasma LDL after oral administration for 14 weeks.[58] We found no differences for plasma triglycerides (Figure 6e), plasma HDL levels (Figure 6f), or the VLDL/LDL-cholesterol–HDL

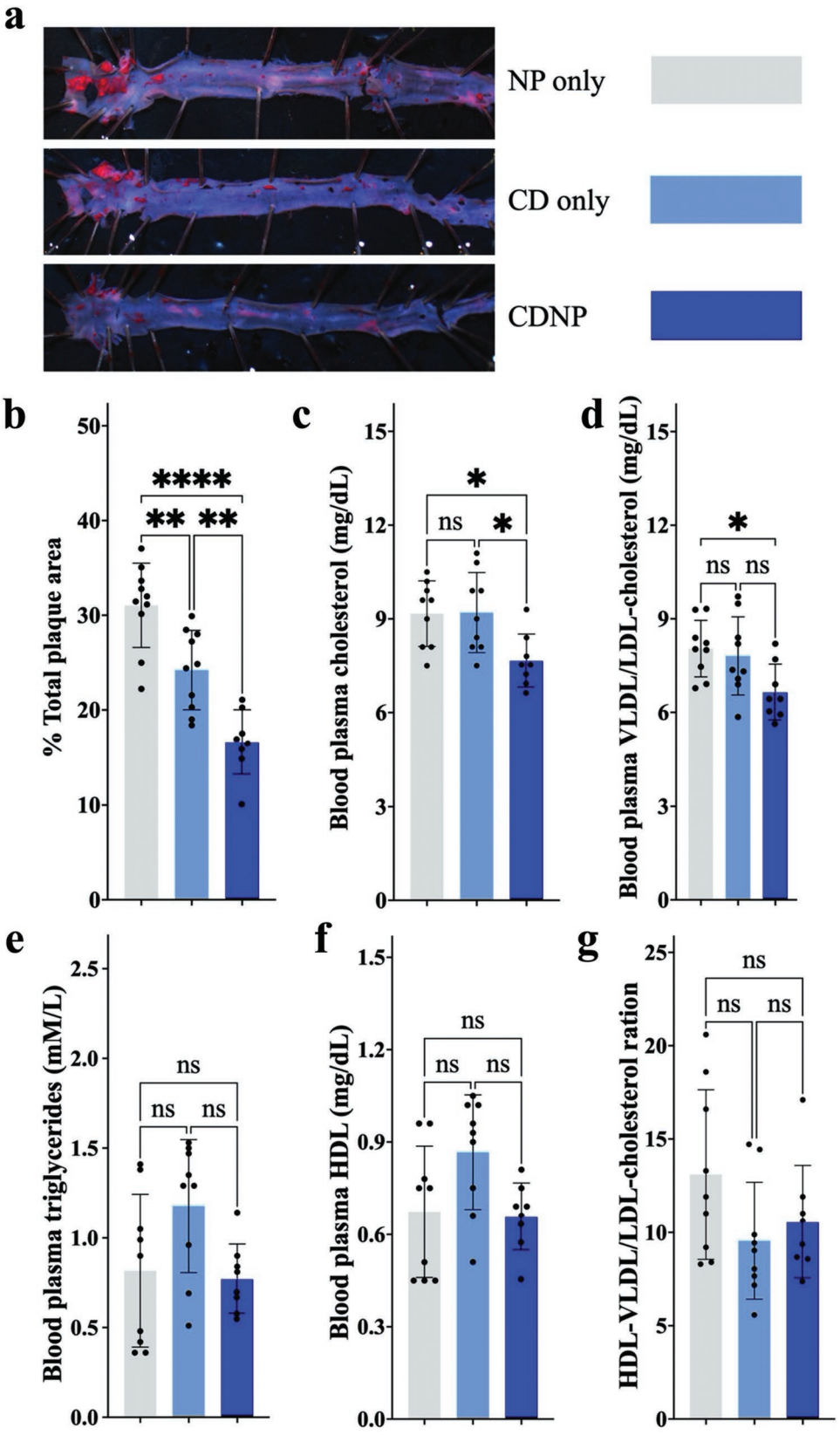

Figure 6. Reduction of atherosclerosis by CDNPs. a) En face Oil Red O-stained aortas treated with NPs only, free CD, and CDNPs; b) Quantification of % plaque volumes from Figure 6a ($n \geq 8$, $^{**}p < 0.01$, $^{****}p < 0.0001$); c–g) Total lipid profiling of blood plasma collected post-treatment with NPs only, free CD, and CDNPs ($n \geq 8$, ns, $^{*}p < 0.05$). Evaluation of outliers was performed using Grubbs' method; no outlier was detected. These assays were analyzed using one-way ANOVA with the Tukey test, comparing all groups. All data are presented as mean ± SD.

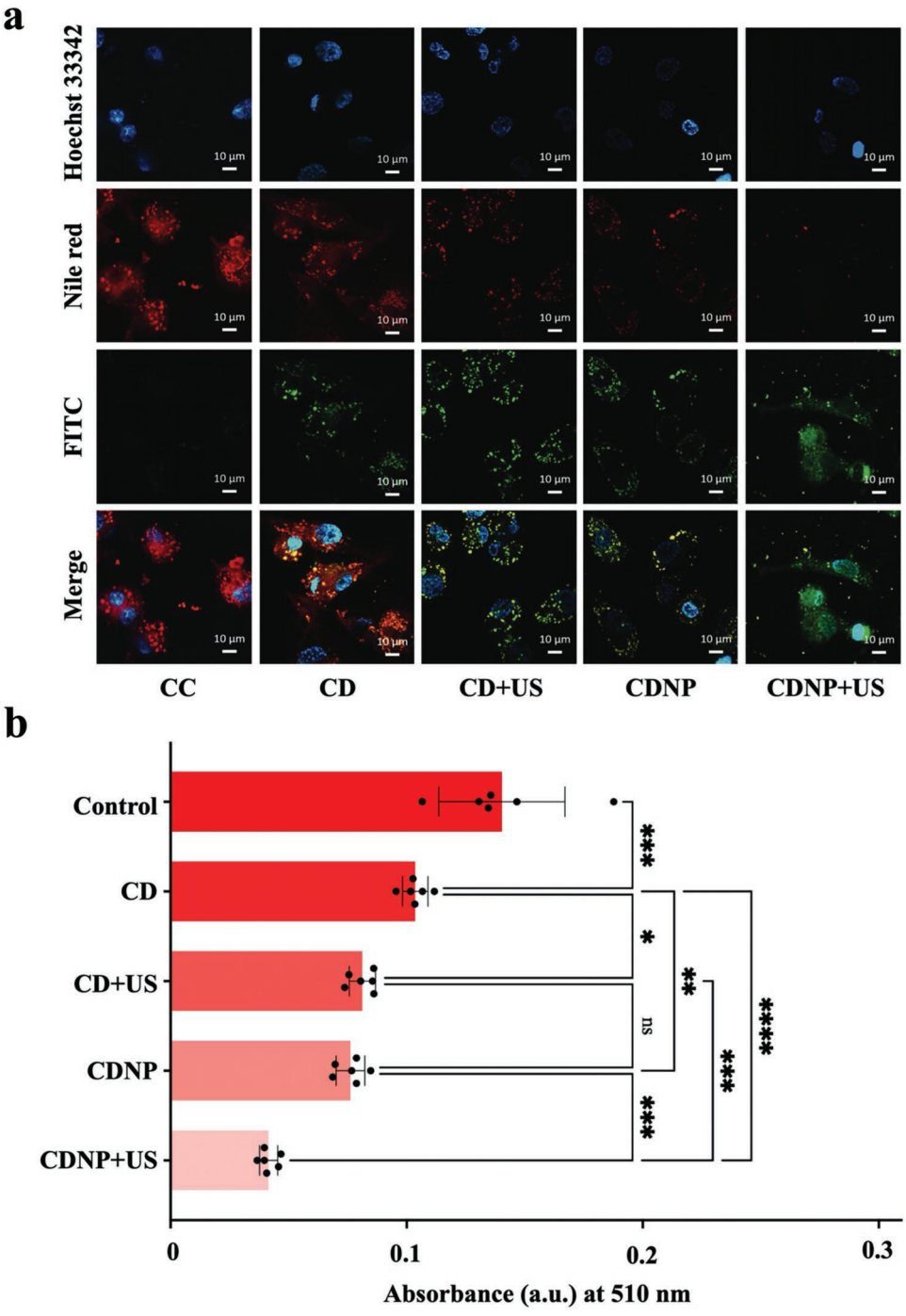

Figure 7. US-triggered CDNPs reduce cholesterol crystals (CCs). a) Cellular uptake of CDNPs in cholesterol-loaded THP-1 macrophages (scale bar 10 μm); b) Quantification of Oil Red O-stained cells treated with US-triggered CDNPs, indicating US triggering of CDNPs reduced CCs (n = 6, ns, $*p < 0.05$, $**p < 0.01$, $***p < 0.001$, $****p < 0.0001$). Evaluation of outliers was performed using Grubbs' method; no outlier was detected. This assay was analyzed using the one-way ANOVA repeated measures with the Tukey test, comparing all groups. All data are presented as mean ± SD.

ratio (Figure 6g). Our in vivo results indicate that the CDNPs facilitated regression of atherosclerosis and reduced levels of cholesterol and VLDL/LDL-cholesterol in blood plasma.

With our convincing in vivo data, we further explored the effect of therapeutic US-triggered CDNPs on the reduction of CCs from THP-1 macrophages. NR-labeled cholesterol crystal (NR-CC)-laden THP-1 macrophages were developed by incubating NR-CC with THP-1 macrophages for 4 h.[22] The NR-CC-loaded THP-1 macrophages were treated with fluorescein isothiocyanate (FITC)-labeled CD or FITC-labeled CDNPs (with and without a US trigger). Therapeutic US parameters were 1 MHz, 2 W cm^{-2}, 50% duty cycle, and 30 s (i.e., 2.97 joules

of US energy per mL of sample), which were lower than previously reported parameters to ensure cell viability.[31,34] Fluorescence microscopy was performed 3 h post-treatment and showed that US triggering improved the cellular uptake of FITC CDNPs (green fluorescence) and reduced the Nile Red staining (red fluorescence) in the cytoplasm of the cells compared with the control groups (**Figure 7**a). This result indicates that with exposure to US, cellular uptake of CDNPs increases[31] and thus attenuates the build-up of lipid deposition, as CD is known to solubilize CCs by forming an inclusion complex.[1] Our data were complemented by the quantification of Oil Red O staining using the absorbance at 510 nm, demonstrating a significant reduction in intensity in the US-triggered CDNP treatment group as compared to controls (Figure 7b). This result confirms that the use of US triggering further improves the anti-atherosclerotic efficacy of CDNPs.

4. Conclusion

We designed and developed nanoparticles using a one-step, sonication-based mini-emulsion method for delivering CD to treat atherosclerosis. The synthesized CDNPs possessed good biocompatibility, did not cause hemolysis, and enhanced the cellular uptake of CD. The CDNPs significantly improved the anti-atherosclerotic efficacy of CD (1.925-fold) compared to free CD in a model of atherosclerosis using ApoE$^{-/-}$ mice fed a high-fat diet. Further, NPs loaded with IR780 showed contrast enhancement in US and NIR imaging and can thus be used as a multimodal contrast agent. Applying a US trigger resulted in improved cellular uptake of CDNPs and increased the efficacy of CD by 1.56-fold as compared to CDNPs alone. Thus, CDNPs could be used as a theranostic agent for intervention in atherosclerosis and potentially other diseases as CD treatment has shown significant therapeutic efficacy in diseases such as Niemann–Pick disease type C and Alzheimer's disease. Because CD, including HPβCD, removes cholesterol molecules from the envelope of viruses, thereby causing disruptions that reduce their infectivity,[59,60] a CD-carrier platform such as CDNPs could potentially be used as an antiviral therapy against various viruses including HIV and SARS-CoV-2 (COVID-19). Furthermore, CDNPs can help reduce adverse effects as they can be used to increase the specificity of CD delivery at the site of disease using a US trigger. Also, CDNPs can be used for the co-delivery of multiple potent drugs. Thus, we believe that CDNPs provide a US trigger-responsive theranostic platform for diagnostic and therapeutic delivery of anti-atherosclerotic therapy.

Supporting Information

Supporting Information is available from the Wiley Online Library or from the author.

Acknowledgements

X.W. and K.P. contributed equally to this work. The authors wish to acknowledge the Industrial Research and Consultancy Centre and Sophisticated Analytical Instruments Facility at the IIT Bombay for providing access to their microscopy facility. Some figures were created with BioRender. S.M. would like to acknowledge the Department of Biotechnology, Government of India, for sponsoring his Ph.D. scholarship. A.P.G.W. and J.P. are supported by Monash University Scholarships. J.P. is also supported by a National Health and Medical Research Council (NHMRC) of Australia Postgraduate Scholarship. Y.J. is supported by a Ph.D. scholarship from the Department of Biotechnology, Government of India. X.W. is supported by a Future Leader Fellowship from the National Heart Foundation of Australia and the Baker Fellowship. K.P. is supported by an L3 Investigator Fellowship from the NHMRC.

Open access publishing facilitated by Monash University, as part of the Wiley - Monash University agreement via the Council of Australian University Librarians.

Conflict of Interest

The authors declare no conflict of interest.

Data Availability Statement

The data that support the findings of this study are available in the supplementary material of this article.

Keywords

atherosclerosis, cyclodextrin, polybutylcyanoacrylate, theranostics, ultrasound imaging

Received: February 14, 2022
Revised: May 24, 2022
Published online: June 16, 2022

[1] S. Zimmer, A. Grebe, S. S. Bakke, N. Bode, B. Halvorsen, T. Ulas, M. Skjelland, D. De Nardo, L. I. Labzin, A. Kerksiek, C. Hempel, M. T. Heneka, V. Hawxhurst, M. L. Fitzgerald, J. Trebicka, I. Björkhem, J.-Å. Gustafsson, M. Westerterp, A. R. Tall, S. D. Wright, T. Espevik, J. L. Schultze, G. Nickenig, D. Lütjohann, E. Latz, *Sci. Transl. Med.* **2016**, *8*, 333ra50.
[2] Y.-C. Chen, A. L. Huang, T. S. Kyaw, A. Bobik, K. Peter, *Arterioscler., Thromb., Vasc. Biol.* **2016**, *36*, e63.
[3] X. Wang, K. Peter, *Arterioscler., Thromb., Vasc. Biol.* **2017**, *37*, 1029.
[4] P. Duewell, H. Kono, K. J. Rayner, C. M. Sirois, G. Vladimer, F. G. Bauernfeind, G. S. Abela, L. Franchi, G. Nunez, M. Schnurr, T. Espevik, E. Lien, K. A. Fitzgerald, K. L. Rock, K. J. Moore, S. D. Wright, V. Hornung, E. Latz, *Nature* **2010**, *464*, 1357.
[5] M. S. Bittencourt, R. J. Cerci, *BMC Med.* **2015**, *13*, 260.
[6] P. Libby, *Am. J. Cardiol.* **2003**, *91*, 4B.
[7] Y.-n. Cao, L. Xu, Y.-c. Han, Y.-n. Wang, G. Liu, R. Qi, *Drug Discovery Today* **2017**, *22*, 180.
[8] R. A. Hegele, S. Tsimikas, *Circ. Res.* **2019**, *124*, 386.
[9] S. Kühnast, M. C. Louwe, M. M. Heemskerk, E. J. Pieterman, J. B. van Klinken, S. A. A. van den Berg, J. W. A. Smit, L. M. Havekes, P. C. N. Rensen, J. W. A. van der Hoorn, H. M. G. Princen, J. W. Jukema, *PLoS One* **2013**, *8*, e66467.
[10] B. L. Sanchez-gaytan, F. Fay, M. E. Lobatto, J. Tang, M. Ouimet, Y. Kim, S. E. M. V. D. Staay, S. M. V. Rijs, B. Priem, L. Zhang, E. A. Fisher, K. J. Moore, R. Langer, Z. A. Fayad, W. J. M. Mulder, **2015**, *26*, 443.

[11] C. Ward Natalie, F. Watts Gerald, H. Eckel Robert, *Circ. Res.* **2019**, *124*, 328.
[12] S. R. Salim Yusuf, S. Ôunpuu, S. Anand, *Circulation* **2001**, *104*, 2746.
[13] M. Flores Alyssa, J. Ye, K.-U. Jarr, N. Hosseini-Nassab, R. Smith Bryan, J. Leeper Nicholas, *Arterioscler., Thromb., Vasc. Biol.* **2019**, *39*, 635.
[14] H. Kim, J. Han, J.-H. Park, *J. Controlled Release* **2020**, *319*, 77.
[15] D. R. Lewis, L. K. Petersen, A. W. York, K. R. Zablocki, L. B. Joseph, V. Kholodovych, R. K. Prud'homme, K. E. Uhrich, P. V. Moghe, *Proc. Natl. Acad. Sci. USA* **2015**, *112*, 2693.
[16] L. Szente, A. Singhal, A. Domokos, B. Song, *Molecules* **2018**, *23*, 1228
[17] A. Singhal, E. S. Krystofiak, W. G. Jerome, B. Song, *Sci. Rep.* **2020**, *10*, 8663.
[18] S. S. Bakke, M. H. Aune, N. Niyonzima, K. Pilely, L. Ryan, M. Skjelland, P. Garred, P. Aukrust, B. Halvorsen, E. Latz, J. K. Damås, T. E. Mollnes, T. Espevik, *J. Immunol.* **2017**, *199*, 2910.
[19] M. Abdur Rouf, I. Vural, E. Bilensoy, A. Hincal, D. D. Erol, *J. Inclusion Phenom. Macrocyclic Chem.* **2011**, *70*, 167.
[20] D. Carradori, H. Chen, B. Werner, A. S. Shah, C. Leonardi, M. Usuelli, R. Mezzenga, F. Platt, J.-C. Leroux, *Small* **2020**, *16*, 2004735.
[21] P. Jansook, N. Ogawa, T. Loftsson, *Int. J. Pharm.* **2018**, *535*, 272.
[22] H. Kim, S. Kumar, D.-W. Kang, H. Jo, J.-H. Park, *ACS Nano* **2020**, *14*, 6519.
[23] Y. Dou, Y. Chen, S. Han, X. Xu, Q. Shi, J. Zhang, J. Guo, Y. Jia, Y. Liu, Y. Deng, X. Li, R. Wang, *J. Controlled Release* **2016**, *235*, 48.
[24] X. Jin, S. Asghar, X. Zhu, Z. Chen, C. Tian, L. Yin, Q. Ping, Y. Xiao, *Colloids Surf., B* **2018**, *162*, 25.
[25] J. N. Blythe, A. Habib, A. Gulati, P. A. Brennan, *Br. J. Oral Maxillofac. Surg.* **2011**, *49*, 486.
[26] R. M. Koffie, C. T. Farrar, L.-J. Saidi, C. M. William, B. T. Hyman, T. L. Spires-Jones, *Proc. Natl. Acad. Sci. USA* **2011**, *108*, 18837.
[27] M. Liu, A. Dasgupta, P. Koczera, S. Schipper, D. Rommel, Y. Shi, F. Kiessling, T. Lammers, *Mol. Pharmaceutics* **2020**, *17*, 2840.
[28] B. Li, R. Aid-Launais, M.-N. Labour, A. Zenych, M. Juenet, C. Choqueux, V. Ollivier, O. Couture, D. Letourneur, C. Chauvierre, *Biomaterials* **2019**, *194*, 139.
[29] L. Appold, Y. Shi, S. Rütten, A. Kühne, A. Pich, F. Kiessling, T. Lammers, *Macromol. Biosci.* **2017**, *17*, 1700002.
[30] G. Dufour, B. Evrard, P. de Tullio, *AAPS J.* **2015**, *17*, 1501.
[31] R. Chandan, R. Banerjee, *Sci. Rep.* **2018**, *8*, 2624.
[32] T. Kyaw, C. Tay, A. Khan, V. Dumouchel, A. Cao, K. To, M. Kehry, R. Dunn, A. Agrotis, P. Tipping, A. Bobik, B.-H. Toh, *J. Immunol.* **2010**, *185*, 4410.
[33] F. Tranquart, M. Arditi, T. Bettinger, P. Frinking, J. M. Hyvelin, A. Nunn, S. Pochon, I. Tardy, *Z. Gastroenterol.* **2014**, *52*, 1268.
[34] A. Prabhakar, R. Banerjee, *ACS Omega* **2019**, *4*, 15567.
[35] J. A.-T. Walker, X. Wang, K. Peter, K. Kempe, S. R. Corrie, *ACS Sens.* **2020**, *5*, 1190.
[36] K. Rajamäki, J. Lappalainen, K. Oörni, E. Välimäki, S. Matikainen, P. T. Kovanen, K. K. Eklund, *PLoS One* **2010**, *5*, e11765.
[37] J. L. Ramírez-Zacarías, F. Castro-Muñozledo, W. Kuri-Harcuch, *Histochemistry* **1992**, *97*, 493.
[38] P. Koczera, L. Appold, Y. Shi, M. Liu, A. Dasgupta, V. Pathak, T. Ojha, S. Fokong, Z. Wu, M. van Zandvoort, O. Iranzo, A. J. C. Kuehne, A. Pich, F. Kiessling, T. Lammers, *J Controlled Release* **2017**, *259*, 128.
[39] N. Behan, C. Birkinshaw, N. Clarke, *Biomaterials* **2001**, *22*, 1335.
[40] M. Danaei, M. Dehghankhold, S. Ataei, F. Hasanzadeh Davarani, R. Javanmard, A. Dokhani, S. Khorasani, M. R. Mozafari, *Pharmaceutics* **2018**, *10*, 57.
[41] M. Stein, E. Hamacher, *Int. J. Pharm.* **1992**, *80*, R11.
[42] C. O'sullivan, C. Birkinshaw, *Polym. Degrad. Stab.* **2002**, *78*, 7.
[43] A. L. Klibanov, J. A. Hossack, *Invest. Radiol.* **2015**, *50*, 657.
[44] Y.-L. Xu, Y.-H. Gao, Z. Liu, K.-B. Tan, X. Hua, Z.-Q. Fang, Y.-L. Wang, Y.-J. Wang, H.-M. Xia, Z.-X. Zhuo, *Int. J. Cardiol.* **2010**, *138*, 182.
[45] X. Wang, E. Hagemeyer Christoph, D. Hohmann Jan, E. Leitner, C. Armstrong Paul, F. Jia, M. Olschewski, A. Needles, K. Peter, I. Ahrens, *Circulation* **2012**, *125*, 3117.
[46] M. Liu, P. Zhang, L. Deng, D. Guo, M. Tan, J. Huang, Y. Luo, Y. Cao, Z. Wang, *Biomater. Sci.* **2019**, *7*, 1132.
[47] J.-W. Muller, R. van Hees, M. van Sambeek, P. Boutouyrie, M. Rutten, P. Brands, M. Wu, R. Lopata, *Biomed. Opt. Express* **2021**, *12*, 4207.
[48] T. Ojha, V. Pathak, N. Drude, M. Weiler, D. Rommel, S. Rütten, B. Geinitz, M. J. van Steenbergen, G. Storm, F. Kiessling, T. Lammers, *Pharmaceutics* **2019**, *11*, 433
[49] R. Chandan, S. M. Mehta, R. Banerjee, *ACS Biomater. Sci. Eng.* **2020**, *6*, 4731.
[50] H. Yuan, H. Hu, J. Sun, M. Shi, H. Yu, C. Li, Y. U. Sun, Z. Yang, R. M. Hoffman, *In Vivo* **2018**, *32*, 1025.
[51] C. Prasad, E. Bhatia, R. Banerjee, *Sci. Rep.* **2020**, *10*, 8587.
[52] R. Challa, A. Ahuja, J. Ali, R. K. Khar, *AAPS PharmSciTech* **2005**, *6*, E329.
[53] E. Sulheim, H. Baghirov, E. von Haartman, A. Bøe, A. K. O. Åslund, Y. Mørch, C. d. L. Davies, *J. Nanobiotechnol.* **2016**, *14*, 1.
[54] H. T. Ta, N. P. Truong, A. K. Whittaker, T. P. Davis, K. Peter, *Expert Opin. Drug Delivery* **2018**, *15*, 33.
[55] S. Feng, L. Nie, P. Zou, J. Suo, *J. Appl. Polym. Sci.* **2015**, *132*, 41431.
[56] J. V. Tapia-Vieyra, B. Delgado-Coello, J. Mas-Oliva, *Arch. Med. Res.* **2017**, *48*, 12.
[57] A. R. Mendelsohn, J. W. Larrick, *Rejuvenation Res.* **2016**, *19*, 252.
[58] E. M. Wagner, K.-L. C. Jen, J. D. Artiss, A. T. Remaley, *Metabolism* **2008**, *57*, 1046.
[59] P. F. Garrido, M. Calvelo, A. Blanco-González, U. Veleiro, F. Suárez, D. Conde, A. Cabezón, Á. Piñeiro, R. Garcia-Fandino, *Int. J. Pharm.* **2020**, *588*, 119689.
[60] R. M. Graham David, E. Chertova, M. Hilburn Joanne, O. Arthur Larry, E. K. Hildreth James, *J. Virol.* **2003**, *77*, 8237.